The Rouse–Mooney model for coherent quasielastic neutron scatterings of single chains well entangled in polymer melts

Y.-H. Lin and C.-F. Huang

Citation: The Journal of Chemical Physics **128**, 224903 (2008); doi: 10.1063/1.2927870
View online: http://dx.doi.org/10.1063/1.2927870
View Table of Contents: http://scitation.aip.org/content/aip/journal/jcp/128/22?ver=pdfcov
Published by the AIP Publishing

The Rouse–Mooney model for coherent quasielastic neutron scatterings of single chains well entangled in polymer melts

Y.-H. Lin[a] and C.-F. Huang
Department of Applied Chemistry, National Chiao Tung University, Hsinchu, Taiwan 30050

(Received 18 February 2008; accepted 22 April 2008; published online 9 June 2008)

The dynamic structure factor (DSF) for single (labeled) chains well entangled in polymer melts has been developed based on the Rouse–Mooney picture; the DSF functions derived from the Langevin equations of the model in both discrete and continuous forms are given. It is shown that for all practical purposes, it is sufficient to use the continuous form to analyze experimental results in the "safe" q region (q being the magnitude of the scattering wave vector $\mathbf{q}$) where the Rouse-segment-based theories are applicable. The DSF form reduces to the same limiting form as that of the free Rouse chain as q^2a^2 or $q^2R^2 \to \infty$ (a and R being the entanglement distance and the root mean square end-to-end distance, respectively), confirming what has been expected physically. The natural reduction to the limiting form allows the full range of DSF curves to be displayed in terms of the reduced Rouse variable $q^2(Z_dt)^{0.5}$ in a unified way. The displayed full range represents a framework or "map," with respect to which effects occurring in different regions of the DSF may be located and studied in a consistent manner. One effect is the significant or noticeable deviations of the theoretical DSF curves from the limiting curve in the region $\sim 4 > q^2(Z_dt)^{0.5} > \sim 0.1$ (a time region where $t < \tau_1^e$) to the faster side as qa is in the range 1–5. This is supported by the comparison of the experimental results of an entangled poly(vinylethylene) sample with the theoretical curves. The DSF functional forms predict plateaus with heights depending on the value of q—q-split plateaus—as can be experimentally observed in the time region greater than the relaxation time τ_1^e of the lowest Rouse–Mooney mode, when qa falls between ~ 1 and ~ 7. High sensitivity of the distribution of the q-split plateaus to a enables its value to be extracted from matching the calculated with the experimental results. The thus obtained a value for a well-entangled poly(ethylene-co-butene) polymer is in close agreement with the rheological result. It is shown that the fixed-end boundary conditions in the Rouse–Mooney model are responsible for the correct prediction of the distribution of the q-split plateaus. © *2008 American Institute of Physics*.
[DOI: 10.1063/1.2927870]

I. INTRODUCTION

Because of the large number of atoms and degrees of freedom in a chain molecule, a polymer is rich in its dynamics, with its relaxation-time distribution covering many decades.[1–5] Various techniques have been used to study different aspects of polymer dynamics. In comparison with the wide range that the viscoelastic-response measurements are capable of probing, the neutron spin-echo spectroscopy for studying the coherent scattering has a narrower time window and is mainly suitable for probing certain aspects of chain dynamics.[6] Successful models have been developed describing the viscoelastic responses quantitatively over the whole range: From the glassy-relaxation region to the flow region.[7–9] The physical pictures as contained in these models may provide the approaches for analyzing the coherent quasielastic (or dynamic) neutron scattering results.

The relaxation modulus $G(t)$ functional forms have been given[7–9] by incorporating a stretched exponential Kohlrausch, Williams, and Watts (KWW) form for the glassy-relaxation process $\mu_G(t)$ into the extended reptation theory[2,10–12] (ERT) (for entangled systems) or the Rouse theory[2,13–16] (for entanglement-free systems) as the frame of reference. The creep compliance $J(t)$ curves[17–19] and viscoelastic spectra $G^*(\omega)$ (Ref. 20) of nearly monodisperse polystyrene melts have been recently[7–9] quantitatively analyzed over the whole range in terms of the $G(t)$ functional forms. From the extensive $J(t)$ and $G^*(\omega)$ line-shape analyses, it is clear that the Rouse modes of motion $\mu_R(t)$ is the only dynamic process following the glassy-relaxation process $\mu_G(t)$ in an entanglement-free system. As entanglements begin to occur with increasing molecular weight, $\mu_R(t)$ is replaced by the Rouse–Mooney modes of motion[2,10–12,21] $\mu_A(t)$—modes of motion of an entanglement strand with both ends fixed—as the first process right after $\mu_G(t)$. The $\mu_A(t)$ process plays an important role in the success of the ERT, quantitatively describing the transition from the glassy-relaxation region to the rubberlike-to-fluid region—the $\mu_X(t) - \mu_B(t) - \mu_C(t)$ region[2,7–12]—in the relaxation modulus $G(t)$.

Concurrently, dynamic neutron scatterings from single (labeled) entanglement-free chains in polymer melts are well described by the Rouse model, if the magnitude of the scattering wave vector q is not too large[6,22] ($q \leqslant \sim 1.5\ \mathrm{nm}^{-1}$ or

[a]Electronic mail: yhlin@mail.nctu.edu.tw.

$qb \leqslant \sim 2$, with b being the typical root mean square length of a Rouse segment, $b=\langle \mathbf{b}^2 \rangle^{0.5}$ for the studied polymers). For $q > \sim 1.5$ nm^{-1}, deviations from the Rouse theory may be due to the segmental interactions within and between "Rouse" segments.[23] In well-entangled systems, the single-chain dynamic scatterings deviate in a characteristic way from being described by the Rouse model even in the $q \leqslant \sim 1.5$ nm^{-1} region. The understandings gained from the studies of the viscoelastic responses $G(t)$, $J(t)$, and $G^*(\omega)$ (Refs. 2 and 7–12) suggest that dynamic scatterings from well-entangled labeled chains may be studied in terms of the Rouse–Mooney model. Restricted to the length scale of an entanglement strand, a, the "static" ("structural") and dynamic properties revealed by the scatterings are expected to be independent of molecular weight. Indeed, experimental results[24] have suggested that the dynamic-scattering line shapes become independent of molecular weight if the molecular weight is sufficiently large—i.e., if the polymer system is extremely well entangled.

II. DYNAMIC STRUCTURE FACTORS OF ROUSE-SEGMENT-BASED MODELS

A. Free chains

The Rouse dynamic behavior is described by the Langevin equation[1,2,25] for a chain consisting of beads connected by springs with the entropic-force constant $3kT/b^2$.[1,2,13,14] Consider a single Rouse chain—labeled in experimental measurements—with N_0 beads, whose positions at time t are denoted by $\{\mathbf{R}_n(t)\}$. With the beads' displacements being sums of Gaussian random steps, the dynamic structure factor (DSF) of the single Rouse chain can be expressed by[1,6]

$$S(\mathbf{q},t) = \frac{1}{N_0}\sum_{n=1}^{N_0}\sum_{m=1}^{N_0}\langle \exp[i\mathbf{q}\cdot(\mathbf{R}_m(t)-\mathbf{R}_n(0))]\rangle = \frac{1}{N_0}\sum_{n=1}^{N_0}\sum_{m=1}^{N_0}\exp\left[-\frac{\mathbf{q}^2}{6}\langle(\mathbf{R}_m(t)-\mathbf{R}_n(0))^2\rangle\right]. \quad (1)$$

In terms of the Rouse normal modes,[1,2] while the DSF derived from Eq. (1) based on the discrete model is given in Appendix A, the one based on the continuous model is given by[1,6]

$$S(\mathbf{q},t) = \frac{1}{N_0}\exp(-\mathbf{q}^2 D_G t)\times\sum_{n=1}^{N_0}\sum_{m=1}^{N_0}\exp\left[-\frac{\mathbf{q}^2}{6}b^2|m-n| - \frac{2\mathbf{q}^2 N_0 b^2}{3\pi^2}\sum_{p=1}^{\infty}\frac{1}{p^2}\cos\left(\frac{mp\pi}{N_0}\right)\cos\left(\frac{np\pi}{N_0}\right)\times\left[1-\exp\left(\frac{-t}{\tau_p}\right)\right]\right], \quad (2)$$

with

$$\tau_p = \frac{\zeta N_0^2 b^2}{3kT\pi^2 p^2} = K\frac{M^2}{3p^2}. \quad (3)$$

In Eq. (3), M is the molecular weight corresponding to N_0 beads per chain, and the frictional factor K is given by (see Appendix B)

$$K = \frac{\zeta b^2}{kT\pi^2 m^2} = \frac{\zeta K_\infty^2}{kT\pi^2 b^2} = \frac{3K_\infty^2}{\pi^2 Z_d}, \quad (4)$$

with m being the mass per Rouse segment. As explained in Appendix B, the frictional factor K serves an equivalent role as the parameter Z_d $(=3kTb^2/\zeta)$ that has often been used to characterize the dynamic neutron scatterings and will be used in the data analyses below.

If the free Rouse chain is trapped inside a domain with a diameter of $\sqrt{N_0}b$, the DSF is obtained from Eq. (2) by setting $D_G=0$:

$$S(\mathbf{q},t) = \frac{1}{N_0}\times\sum_{n=1}^{N_0}\sum_{m=1}^{N_0}\exp\left[-\frac{\mathbf{q}^2}{6}b^2|m-n| - \frac{2\mathbf{q}^2 N_0 b^2}{3\pi^2}\sum_{p=1}^{\infty}\frac{1}{p^2}\cos\left(\frac{mp\pi}{N_0}\right)\cos\left(\frac{np\pi}{N_0}\right)\times\left[1-\exp\left(\frac{-t}{\tau_p}\right)\right]\right]. \quad (5)$$

Eq. (5) will be used in Sec. VI.

B. Entanglement strands

Here, we consider an *extremely* well-entangled system in which both the labeled chains and the matrix chains are very long with molecular weights much greater than the entanglement molecular weight M_e. In other words, $N=N_0/N_e \gg 1$, with N_0 denoting the number of Rouse segments of a chain and N_e denoting the number of Rouse segments per entanglement strand. Consider an entanglement strand of a labeled chain in the system. We picture that the first bead $\mathbf{R}_1(t)$ is connected to the *fixed* origin $\mathbf{O}$ of a chosen coordinate system by a bond vector $\mathbf{b}_0(t)$ and the last bead $\mathbf{R}_{N_e}(t)$ is *fixed* at such a position $\mathbf{R}_e$ that statistically $\langle \mathbf{R}_e^2 \rangle = N_e b^2 = a^2$, where a is referred to as the entanglement distance or length. Entanglement strands are linked one after another, each with its end-to-end vector $\mathbf{R_e}$ randomly oriented.[1,2,26] If the representative entanglement strand defined above stands for a particular one in the sequence, the origin $\mathbf{O}$ is equivalent to the position of the last bead of the preceding entanglement stand and $\mathbf{R}_{N_e}(t)$ is equivalent to the origin of the next entanglement strand. In this way, beads on each entanglement strand of a chain are counted in an equivalent manner.

As $N \gg 1$, in the timescales as typically probed by the neutron spin-echo spectroscopy—with a properly chosen temperature—entanglement points may be regarded as fixed as the chain does not have the chance to slip through the links (the slip links of the Doi–Edwards model[1,2,26]). Then as shown in Appendix C, under the condition $R \gg q^{-1}$, the DSF of the labeled chain can be expressed as

$$S(\mathbf{q},t)=\frac{1}{N_e}\sum_{n=1}^{N_e}\sum_{m=1}^{N_e}\langle\exp[i\mathbf{q}\cdot(\mathbf{R}_n(t)-\mathbf{R}_m(0))]\rangle$$
$$=\frac{1}{N_e}\sum_{n=1}^{N_e}\sum_{m=1}^{N_e}\exp\left[-\frac{\mathbf{q}^2}{6}\langle(\mathbf{R}_m(t)-\mathbf{R}_n(0))^2\rangle\right], \quad (6)$$

where the Gaussian property of the beads' movements has been used. Although the term with $n=m=N_e$ in Eq. (6) being independent of time does not represent a Gaussian dynamic process, with respect to it, the second equality in Eq. (6) remains valid.

Equation (6) is referred to as the Rouse–Mooney model of coherent quasielastic scattering. In terms of the normal modes,[2,27] while the DSF derived from Eq. (6) based on the discrete model is given in Appendix A, the one based on the continuous model is given by

$$S(\mathbf{q},t)=\frac{1}{N_e}\times\sum_{n=1}^{N_e}\sum_{m=1}^{N_e}\exp\left[-\frac{\mathbf{q}^2}{6}b^2|m-n|\right.$$
$$-\frac{2\mathbf{q}^2N_eb^2}{3\pi^2}\sum_{p=1}^{\infty}\frac{1}{p^2}\sin\left(\frac{mp\pi}{N_e}\right)\sin\left(\frac{np\pi}{N_e}\right)$$
$$\left.\times\left[1-\exp\left(\frac{-t}{\tau_p^e}\right)\right]\right], \quad (7)$$

with

$$\tau_p^e=\frac{\zeta N_e^2b^2}{3kT\pi^2p^2}=K\frac{M_e^2}{3p^2}. \quad (8)$$

There are two main differences between Eqs. (2) and (7) in form: First, the diffusion factor is absent from Eq. (7), reflecting that the chain does not diffuse due to the entanglement points being fixed as assumed. Second, because of the changes in the boundary conditions, cosines in Eq. (2) [or Eq. (5)] are replaced by sines in Eq. (7) (taking N_0 as corresponding to N_e). While the diffusion motion does not occur in either Eq. (5) or (7), the former is for a chain with both ends free while the latter is for a strand with both ends fixed. As explained in Appendix D, for $\mathbf{q}^2N_eb^2\gg1$, Eq. (7) in the short-time region ($t\ll\tau_1^e$) reduces to the same limiting form [Eq. (D3)] as the one that is obtained from Eq. (2) or (5) for $\mathbf{q}^2N_0b^2\gg1$ in the equivalent way.

One may obtain the self-correlation function—as can be probed by incoherent scattering—from Eq. (7) by setting $n=m$. In the time region $t\ll\tau_1^e$, the exponent is dominated by the terms with large p. By replacing $\sin^2(np\pi/N_e)$ by the average $\frac{1}{2}$ and converting the summation over p into integration, one obtains

$$S_{\text{self}}(\mathbf{q},t)=\exp\left[-\frac{q^2N_eb^2}{3\pi^2}\int_0^{\infty}\frac{1}{p^2}\left[1-\exp\left(\frac{-tp^2}{\tau_1^e}\right)\right]dp\right]$$
$$=\exp\left[-\left(\frac{tZ_dq^4}{9\pi}\right)^{1/2}\right]. \quad (9)$$

Equation (9) is identical to the one that is obtained from Eq. (2) for the time region $t\ll\tau_1$ in the equivalent way[1,6]—in the case of from Eq. (2), replacing $\cos^2(np\pi/N_0)$ by the average $\frac{1}{2}$. Thus, even though in the literature the equation [Eq. (9)] used to analyze the short-time incoherent scattering data of entangled systems has been understood (or regarded) as originating from the Rouse theory [Eq. (2)],[6] the analysis-obtained results are equally applicable here—i.e., from the perspective of the Rouse–Mooney model.

III. APPLICABLE q REGION FOR ROUSE-SEGMENT-BASED THEORIES

Before we analyze experimental results in terms of the Rouse and Rouse–Mooney models given above, it is advisable to point out some recent developments in the understanding and characterization of the Rouse or "Rouse" segment based on Monte Carlo simulations on entanglement-free Fraenkel chains.[28,29] It has been concluded that the entropic-force constant on each segment is not a required element to give rise to the Rouse modes of motion in $G(t)$ of an entanglement-free system. As the Fraenkel segment with a sufficiently large force constant can be regarded as basically equivalent to the Kuhn segment as far as the chain conformation is concerned, this conclusion has provided an explanation resolving the paradox that the molecular weights of the Rouse segments and Kuhn segments, m and M_K, are of the same order of magnitude.[30] Thus, the "Rouse" segment having a finite size can be determined experimentally—in general much greater than a chemical segment; for instance, $m=850$ for polystyrene and $m=200-260$ for polyisobutylene,[30–32] the entropic (rubbery) aspects of polymer viscoelasticity in reality are not directly related to the entropic-force constant of the Rouse segment. In spite of this, the Rouse-segment-based molecular theories can still be profitably used in analyzing experimental results. The wide use of the Rouse-segment-based molecular viscoelastic theories can be attributed to two main reasons: One is that their equations of motion are solvable analytically[1,2,10,13,14] and the other is the success of the theories in interpreting experimental results—over the entropic region of viscoelastic response. Here, we take a similar practical view of using the Rouse-segment-based DSF functional forms given in this report. Because the "Rouse" segment has a finite size, the Z_d values, although still extractable from analyses in terms of these DSF functional forms, will eventually cease to be independent of q when q is sufficiently large. Thus, for safe use of the DSF functional forms, one needs to adhere to the criterion that the Z_d values extracted from the experimental DSF data at different q values are in agreement with each other.

In Fig. 1, DSF curves of an entanglement-free polyisobutylene (PIB) sample [$M_n=3870$ and $M_w/M_n=1.05$ (Ref. 22)] at different q values are compared to the results calculated by substituting $N_0=15$ and $b=1.255$ (Ref. 30) into Eq. (A1) and by substituting $N_0=200$ and $b=0.3323$ into Eq. (2)—the values of the N_0 and b are chosen such that $R^2=K_\infty M=N_0b^2=22.06$ nm^2 is maintained.[2,22,33] Failure of the Rouse model at large q being expected, in the comparison between theory and experiment, a Z_d value is chosen by matching the calculated and measured curves at as many low q values as possible. The close matching between theory and

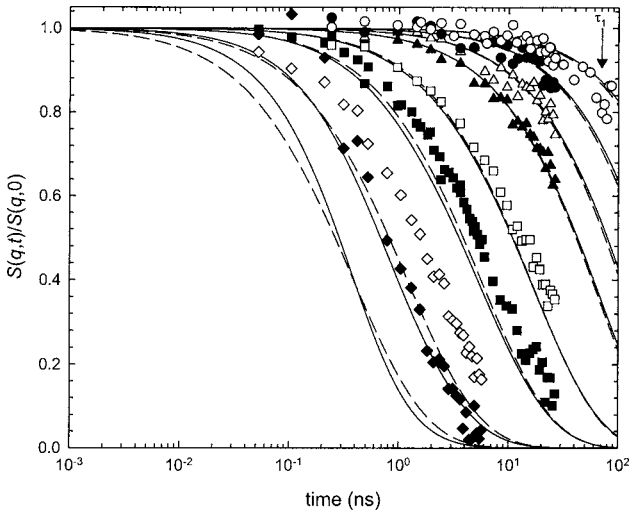

FIG. 1. Comparison of the measured normalized DSF results (○, ●, △, ▲, □, ■, ◇, and ◆ at q=0.4, 0.6, 0.8, 1.0, 1.5, 2.0, 3.0, and 4.0 nm^{-1}, respectively) of the PIB sample with the curves calculated from the Rouse model: (—) from the discrete form, Eq. (A1) (with N_0=15 and b=1.255 nm, giving R^2=22.06 nm^2); (---) from the continuous form, Eq. (2) (with N_0=200 and b=0.3323 nm, giving R^2=22.06 nm^2). The comparison is made with Z_d=0.808 nm^4 ns^{-1}; the arrow marks the position of τ_1.

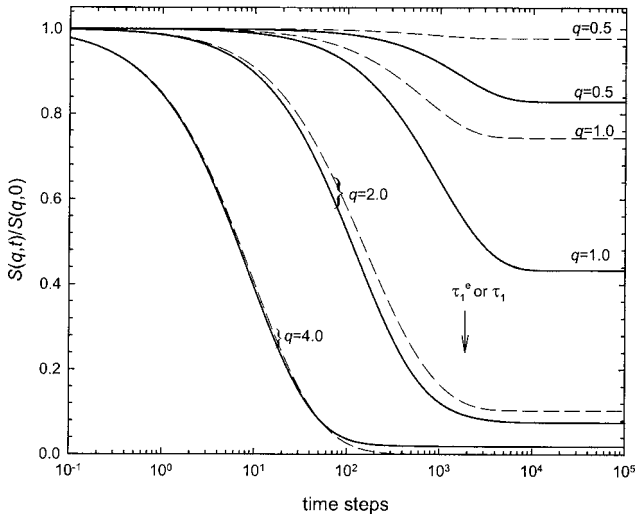

FIG. 2. Normalized DSF curves calculated from Eq. (7) for entanglement strands (both ends fixed; with N_e=100 and b=0.5, giving a=5) are shown as solid lines at the indicated q values. For comparison, the corresponding curves calculated from Eq. (5) for free chains (with N_0=100 and b=0.5) trapped in a domain of diameter a=5 are shown as dashed lines. The arrow marks the position of τ_1^e [for Eq. (7)] or τ_1 [for Eq. (5)].

experiment at the $q<1.5$ nm^{-1} region with a small difference at q=1.5 nm^{-1} is made with the same Z_d value (0.808 nm^4/ns) as used by Richter *et al.*[22] In the $q\leqslant 1.5$ nm^{-1} region, the curves calculated from Eqs. (A1) and Eq. (2) agree well with each other. Thus, for all practical purposes, the continuous model may be used for comparison with the experimental results in the region $q\leqslant 1.5$. This region may be regarded as the applicable or safe region of the Rouse theory. The justification for using the continuous Rouse model in the safe q region does not mean that the chain section that can be assigned as a Rouse or "Rouse" segment is very small. The N_0 and b values chosen for substituting into Eq. (2) are merely some convenient numbers arbitrarily chosen (also see Appendix B). We have found that as long as $R^2=N_0b^2$ is maintained, virtually no difference can be observed between the calculated DSF curves with different N_0 values greater than 50 except at large q values (3.0 and 4.0 nm^{-1}). The above discussion also confirms the practice in the literature where the continuous form has always been used in analyzing neutron spin-echo data in the safe q region.

Equations (2) and (7) are both developed from the same basis using the Rouse segment as the basic structural unit. The Rouse segment lengths b estimated for the polymers studied in this paper are of the same order of magnitude (1.25–1.4 nm). Thus, the region $q\leqslant\sim 1.5$ nm^{-1}, where successful comparison between Eq. (2) and experiment is made in Fig. 1, can also be regarded as the safe q region for evaluating the success of Eq. (7). All the analyses done below for the entangled systems, except for the result of the poly(vinylethylene) (PVE) sample at q=1.79 nm^{-1}, basically fall in the safe region. Although small differences between Eqs. (A5) and (7) can be noticed in the calculated curves [over the plateau region for the poly(ethylene-co-butene) (PEB-2) system studied below], the differences are much smaller than the noise of the data.

IV. ENTANGLEMENT-RELATED CHARACTERISTICS IN THE DSF LINE SHAPES

Equation (7) gives rise to unique DSF line shapes because of the existence of entanglement with a characteristic length a. When the scattering wave vector $\mathbf{q}$ is of such magnitude that $\sim 10>qa>\sim 1$, two characteristics can be identified in the DSF line shapes, as shown in Fig. 2. One occurs in the time region, $t>\tau_1^e$; the other in the $t<\tau_1^e$ region. By emphasizing these characteristics in analyzing the experimental results in terms of Eq. (7), one may effectively extract the value of a. To illustrate these two characteristics in perspective, the DSF line shapes calculated from Eq. (7) at q=0.5, 1, and 2 and shown in Fig. 2 are displayed in Fig. 3 as a function of the reduced Rouse variable $q^2(Z_dt)^{1/2}$.

As shown in Appendix D, under the condition $qa\gg 1$, Eq. (7) in the time region $t\ll\tau_1^e$ reduces to the limiting form, Eq. (D3),[1,34] which is a universal function of the reduced variable $q^2(Z_dt)^{1/2}$. As the condition is changed from $qa>10$ to $qa>1$, obvious plateaus occur in the time region $t>\tau_1^e$, whose heights depend on the value of qa. The way that the q-split plateaus are distributed is sensitive to the value of a—as indicated by $S(\mathbf{q},t\gg\tau_1^e)/S(\mathbf{q},0)$=0.83 at qa=2.5 vs $S(\mathbf{q},t\gg\tau_1^e)/S(\mathbf{q},0)$=0.075 at qa=10. This unique relationship enables the entanglement distance a to be obtained from matching the calculated and measured plateau heights at different q values *simultaneously*.

The other characteristic occurring in the region $t<\tau_1^e$ is relatively subtle, requiring some careful explanations. As shown in Fig. 3, the DSF at q=0.5 or qa=2.5 deviates in the region of $\sim 3>q^2(Z_dt)^{0.5}>\sim 0.2$ from the limiting form [Eq. (D3)] to the faster side. Similarly significant or noticeable deviations occur as qa falls between ~1 and ~5; here, we use the deviation at qa=2.5 as a representative case for explanation.

Imagine an "experimental" system of very high molecular weight, where entanglements could be "switched on and

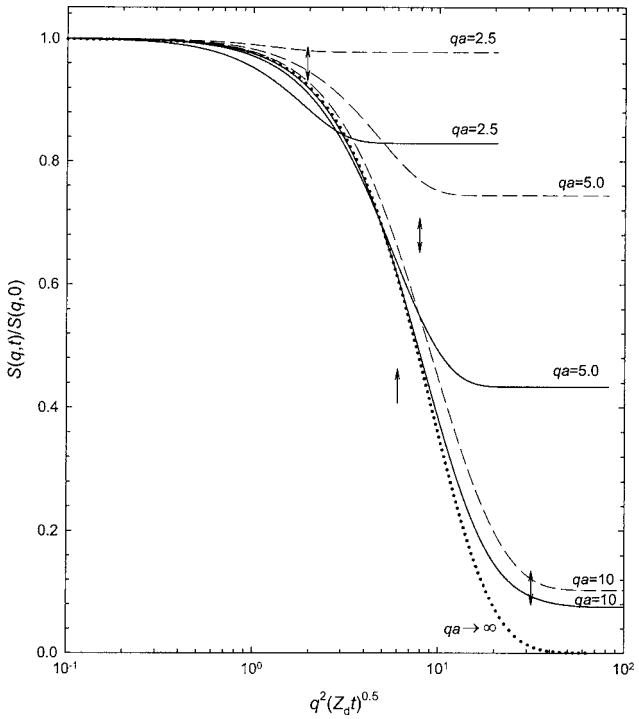

FIG. 3. Normalized DSF curves equivalent to those shown in Fig. 2 at $q=0.5$, 1, and 2 (or $qa=2.5$, 5, and 10) expressed as a function of the reduced Rouse variable $q^2(Z_dt)^{0.5}$ [solid lines calculated from Eq. (7); dashed lines from Eq. (5)]. Also shown is the limiting curve calculated from Eq. (D3) (dotted line). The double-headed arrows mark the positions of $q^2(Z_d\tau_1^e)^{1/2}=q^2(Z_d\tau_1)^{1/2}=q^2a^2/\pi$, while the upward arrow indicates the position of $q^2(Z_d\tau_q)^{1/2}=6$.

off:" If entanglement is on, the system is extremely well entangled—thus, both ends of each entanglement strand can be assumed as fixed—and its entanglement distance a is assumed such that $qa=2.5$. If entanglement is off, the dynamic behavior of the system is described by the Rouse theory under the condition $qR \gg 1$. In the entanglement-free situation, because $qR \gg 1$, the DSF over the short-time region is well described by Eq. (D3). As entanglement is switched on, due to the imposition of the condition $qa=2.5$, the above described deviation from Eq. (D3) shows up. Such a deviation is expected to be observed by monitoring the *apparent* Z_d values that can be extracted from comparing the experimental curves at $qa=2.5$ with Eq. (D3). In the entanglement-free situation, the apparent Z_d values at different q values should be the same as $qR \gg 1$ in all cases. In comparison, the apparent Z_d value in the entangled situation should be larger due to the deviation from Eq. (D3) to the faster side at $qa=2.5$ (Fig. 3). Here, we have assumed that the line shapes at $qa=2.5$ in the region $\sim 3 > q^2(Z_dt)^{0.5} > \sim 0.2$ is sufficiently similar to that of Eq. (D3); in other words, they can be closely superposed on each other by a horizontal shift. Such an assumption, in actual analyses of experimental data,[6,35,36] could be easily practiced without knowing about it because small differences could be easily buried in the noise of neutron spin-echo data. For this reason, the obtained Z_d value is referred to as an apparent one. The above discussion of the existence of deviation from the limiting form [Eq. (D3)] will be illustrated by comparing the results of an entangled PVE sample[36] with the theoretical curves below.

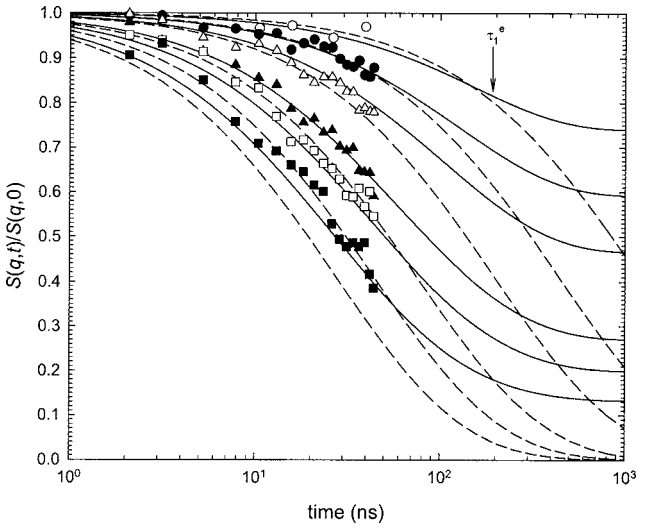

FIG. 4. Comparison of the measured normalized DSF results (○, ●, △, ▲, □, and ■ at $q=0.69$, 0.89, 1.06, 1.38, 1.55, and 1.79 nm^{-1}, respectively) of the PVE sample with the curves (—) calculated from Eq. (7) (with $Z_d=0.2214$ nm^4 ns^{-1} and the combination of $N_e=100$ and $b=0.453$ nm, giving $a=4.53$ nm); with the curves (---) calculated from Eq. (D3) (as done by Richter *et al.*[36] with $Z_d=0.28$ nm^4 ns^{-1}). The arrow marks the position of τ_1^e.

V. COMPARISON OF THEORY AND EXPERIMENT

Neutron spin-echo results of two entangled systems reported in literature will be compared to the theoretical curves calculated from Eq. (7): The PVE sample [$M_w=8.0\times10^4$ or $M_w/M_e\approx20$; $M_w/M_n=1.02$ (Ref. 36)] and the PEB-2 with two ethyl branches per 100 carbons) sample [$M_w=1.9\times10^5$ or $M_w/M_e\approx195$; $M_w/M_n<1.02$ (Ref. 24)]. The PVE system is for testing Eq. (7) over the region from $t \ll \tau_1^e$ to $t<\tau_1^e$, while the PEB-2 system is for testing Eq. (7) over the region from $t \leqslant \tau_1^e$ to $t>\tau_1^e$.

A. Lack of a common short-time region

As pointed out above, based on Eq. (7), DSF curves with different qa in the range 1–5 do not share a common curve in the region of $\sim 4 > q^2(Z_dt)^{0.5} > \sim 0.1$. However, in the literature, the neutron spin-echo data in this region have often been treated as all following Eq. (D3).

In Fig. 4, the neutron spin-echo results of the PVE sample are compared to the curves calculated from Eq. (7) at different q values (ranging from $q=0.69$ to 1.79 nm^{-1} or from $qa=3.13$ to 8.11 using the rheological value $a=4.53$ nm in the calculations).[2,33] In the calculation for a continuous model, the combination of $N_e=100$ and $b=0.453$ nm may be arbitrarily chosen as long as $a=4.53$ nm is maintained. With the same Z_d value (0.2214 nm^4/ns), simultaneous close agreements between experimental results and theoretical curves at different q values appear to be obtainable. Also shown in Fig. 4 is the comparison with the curves calculated from Eq. (D3) as made by Richter *et al.* with $Z_d=0.28$ nm^4/ns:[36] While experimental results are in close agreement with the calculated curves at the small q values (0.69, 0.89, and 1.06 nm^{-1}), significant differences at the large q values (1.38, 1.55, and 1.79 nm^{-1}) can be clearly observed. Thus, in the approach of Richter *et al.*, different (apparent) Z_d values have to be used

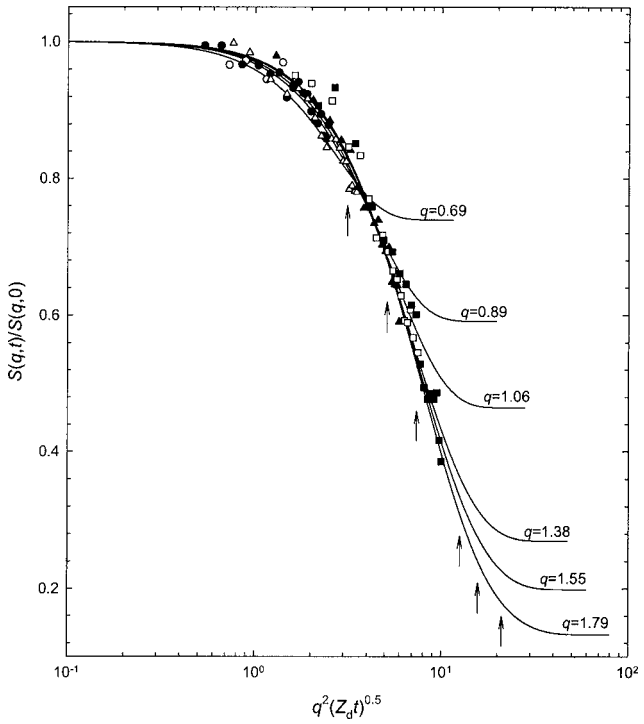

FIG. 5. Comparison of the measured normalized DSF results (the same as in Fig. 4) of the PVE sample with the curves (—) calculated from Eq. (7) (the same as in Fig. 4), both expressed as a function of the reduced Rouse variable, $q^2(Z_d t)^{1/2}$. The arrows from the top to the bottom mark the positions of $q^2(Z_d\tau_1^e)^{1/2}=q^2a^2/\pi$ at $q=0.69$, 0.89, 1.06, 1.38, 1.55, and 1.79 nm^{-1}, respectively.

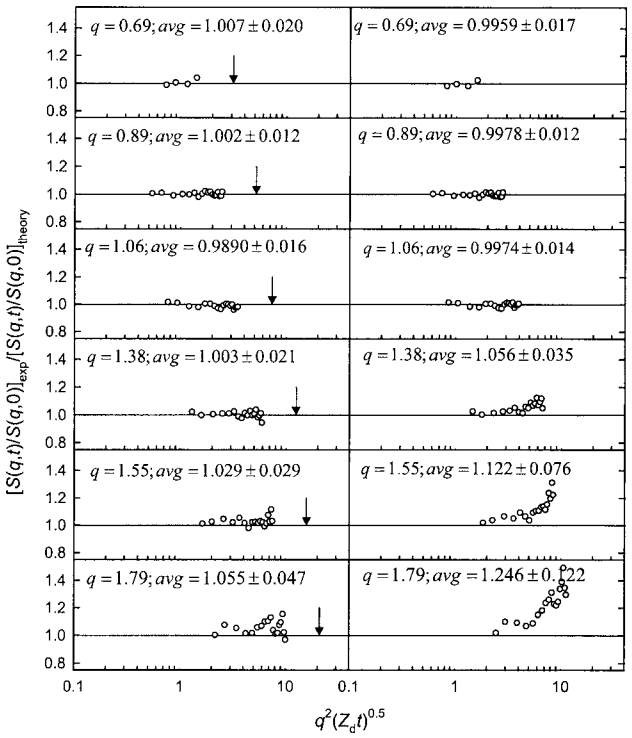

FIG. 6. The ratios of the normalized DSF data of the PVE sample to the values calculated from Eq. (7) (the left panel; the same as in Fig. 5) vs the ratios of the same data to the values calculated from Eq. (D3) (the right panel; the same as in Fig. 4). The arrows (in the left panel) mark the positions of $q^2(Z_d\tau_1^e)^{1/2}=q^2a^2/\pi$.

to achieve agreements with Eq. (D3) at different q values as opposed to the same Z_d being used in obtaining the shown simultaneous agreements with Eq. (7). To further illustrate the subtleness regarding the discussed deviations from Eq. (D3), we show both the experimental results and the curves calculated from Eq. (7) as a function of the reduced Rouse variable $q^2(Z_d t)^{1/2}$ in Fig. 5. In the $3\sim4>q^2(Z_d t)^{0.5}>0.2$ region, the experimental data points, though somewhat noisy, can be observed to shift to the faster side at smaller qa as the calculated curves do. To account for statistical noise, we carried out a more careful analysis of the experimental results as described in the following:

In analyzing any set of DSF results here, clearly two factors need to be considered: (1) The effect of entanglement if the molecular weight is greater than M_e and (2) the failure of a Rouse-segment-based theory [either Eq. (2) or (7)] at sufficiently large q values as shown in Fig. 1. The deviation of Eq. (7) from Eq. (D3) is an issue of entanglement. The agreements between the data points and the theoretical curves can be expressed in terms of the ratios of the experimental values to the calculated values; a perfect correlation is indicated by the ratio of 1. The correlations between the data points and Eq. (7) (with $Z_d=0.2214$ nm^4/ns as determined presently) at different q values are compared to those based on Eq. (D3) (with $Z_d=0.28$ nm^4/ns as determined by Richter *et al.*) in Fig. 6. In general, for the comparison with Eq. (7), one would show the ratio distribution by adjusting the Z_d value such that the average of the ratio values at different q values is 1. However, at $q=1.55$ and 1.79 nm^{-1}, Eq. (7) may be at the borderline of failure of a Rouse-segment-based theory that becomes serious at larger q (Fig. 1). Thus, the ratio distribution shown in Fig. 6 is presented in such a way that the average of the ratio values at the four smaller q values is 1—the Z_d value as used in the comparison of experiment and theory shown in Figs. 4 and 5 has been determined this way. This allows room for deviations from Eq. (7) at $q=1.55$ and 1.79 nm^{-1} to show up if noticeable failure of the Rouse-segment-based theory exists. As opposed to the large deviations at $q=1.38$, 1.55, and 1.79 nm^{-1} in the case of comparing with Eq. (D3) (right panel of Fig. 6), one observes close correlations in the case of comparing with Eq. (7) with only small noticeable deviations at $q=1.55$ and 1.79 nm^{-1} (left panel of Fig. 6). These small deviations are of magnitude similar to those that can be observed in a similar comparison—under the same condition that the average of the ratio values at the four smaller q values is 1—between the data of the PIB sample and Eq. (2) at similar q values (1.5–2 nm^{-1}) and over the same ranges of $q^2(Z_d t)^{0.5}$ as shown in Fig. 7. Furthermore, the value $Z_d=0.2214$ nm^4/ns obtained from matching the DSF curves with Eq. (7) is in close agreement with the values [$Z_d=0.238(\pm20\%)$ (Ref. 37)] obtained from analyzing the incoherent neutron scattering results of the protonated sample in terms of Eq. (9). The existence of deviation from the limiting form is also indicated by the Z_d value (0.28 nm^4/ns) obtained by Richter *et al.* at the three lowest q values (Fig. 4) being significantly larger than these two mutually consistent values.

The above analyses support that Eq. (7) is as valid for an

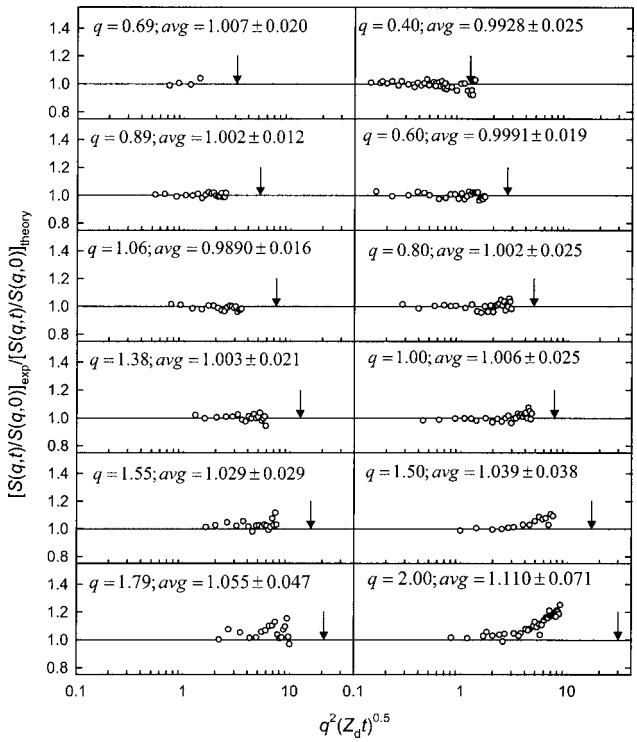

FIG. 7. Comparison of the ratios of the normalized DSF data of the PVE sample to the values calculated from Eq. (7) (the left panel; the same as in Fig. 6) and the ratios of the data of the PIB sample to the values calculated from Eq. (2) (the right panel) at similar q values and over similar ranges of $q^2(Z_d t)^{1/2}$. The arrows mark the positions of $q^2(Z_d\tau_1^e)^{1/2}=q^2a^2/\pi$ (in the left panel) and $q^2(Z_d\tau_1)^{1/2}=q^2R^2/\pi$ (in the right panel).

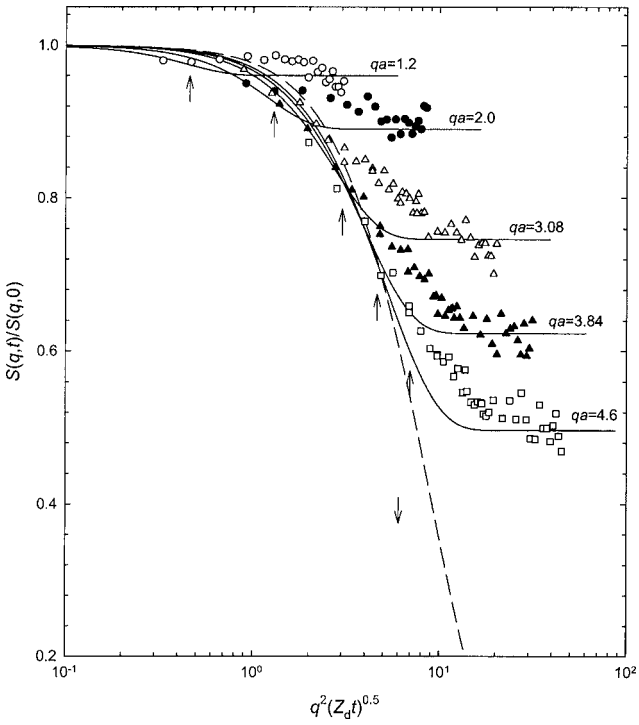

FIG. 8. Comparison of the normalized DSF results (○, ●, △, ▲, and □ at q=0.3, 0.5, 0.77, 0.96, and 1.15 nm^{-1}, respectively) of the PEB-2 sample with the curves calculated from Eq. (7) (with the combination of N_e=100 and b=0.4 nm, giving a=4 nm), both expressed as a function of the reduced Rouse variable, $q^2(Z_d t)^{1/2}$. The comparison is made with Z_d=7 nm^4 ns^{-1}. The upward arrows from the top to the bottom mark the positions of $q^2(Z_d\tau_1^e)^{1/2}=q^2a^2/\pi$ at q=0.3, 0.5, 0.77, 0.96, and 1.15 nm^{-1}, respectively. The limiting curve for $qa\to\infty$ [Eq. (D3)] is shown as the dashed line; the downward arrow indicates the position of $q^2(Z_d\tau_q)^{1/2}=6$.

entangled system as Eq. (2) is for an entanglement-free system as far as the $t<\tau_1^e$ region is concerned. In other words, the comparison of the data of the PVE sample with Eq. (7) supports the existence of deviation from the limiting form in the range $5>qa>1$ as discussed in Sec. IV. This conclusion does not support the observation of the crossover from α relaxation to Rouse dynamics claimed by Richter *et al.*[36] on the basis of the q dependence of the Z_d values obtained from their analyses in terms of Eq. (D3).

We have used the rheological value of a in Eq. (7) to calculate the curves for the PVE sample shown in Figs. 4–7. As the $t\ll\tau_1^e$ to $t<\tau_1^e$ region is not very sensitive to a small change in a, using a value larger by 20% as shown possible by monitoring the q-split plateaus below does not lead to a different conclusion.

B. q-split plateaus

The dependence on the entanglement length a is not as strong in the time region $t<\tau_1^e$ as in the $t>\tau_1^e$ region, where the q-split plateaus occur. By monitoring the agreement between experiment and theory regarding the q-split plateaus, one may adjust the a value to be substituted into Eq. (7). In Fig. 8, the neutron spin-echo results of the PEB-2 sample at 509 K are compared to the curves calculated from Eq. (7) using a=4.0 nm, which is about 16% greater than the rheological value of 3.44 nm obtained at 413 K.[2,33] The comparison is made with Z_d=7 nm^4/ns, which is quantitatively consistent with the incoherent scattering results.[38] Under this condition, there are four features in the shown comparison between theory and experiment: (1) In the short-time region, the data points at different q values "group" together in the same region as the curves calculated from Eq. (7). Because there are too few data in the short-time region, the deviations of Eq. (7) from Eq. (D3) in the region cannot be assessed in this case as in the case of the PVE sample. However, within the noises of the data points, the experimental results are not in disaccord with the analyses of the results of the PVE sample given above. (2) The positions in time of the steep declines as clearly identifiable at the q values: 0.96 and 1.15 nm^{-1} are in close agreement with the theoretical predictions. (3) The heights of the plateaus and their distribution in the long-time region $t>\tau_1^e$ as a function of q are well predicted by the theory. The plateau height level depends on the unitless quantity qa only. The large separation between the two plateaus at the two largest q values (0.96 and 1.15 nm^{-1}) corresponds to a change that can be caused by an ~20% difference in the a value if q is kept the same. Thus, the close matching of the q-split plateau distribution between experiment and Eq. (7) represents a high-resolution determination of the a value. (4) At different q values, the general positions of turning from a steep decline to a plateau are in agreement with the predictions of Eq. (7), despite the noise associated with the data points. The turns are sharper in the theoretical curves than in the experiment results. In a consistent and systematic way at different q values, the experimental values deviate from the calculated curves to the higher side around

the bending point; the data points converge with the calculated plateaus at long times. The above listed features indicate that the Rouse–Mooney model as presented in this paper has captured the basic elements of the mechanism for the relaxation of the DSF curves and their converging to a plateau. The systematic deviations are most likely due to less-than-perfect validity of the model. As shown in Fig. 8, the bending points occur at times longer but not much longer than $t=\tau_1^e$, and higher experimental values start to appear at the timescales of τ_1^e. These deviations from the theoretical curves suggest that any improvement on the model should affect the slowest mode of the Rouse–Mooney process most, lengthening its effective relaxation time.

From the line-shape analyses of viscoelastic responses $G(t)$ and $G^*(\omega)$ in terms of the ERT,[2,7–12] it is known that the chain-slippage (through entanglement links) process $\mu_X(t)$ is responsible for the decline in modulus right after the end of the Rouse–Mooney process $\mu_A(t)$. Due to the relaxation of $\mu_X(t)$, the modulus drops from $\rho RT/M_e$ [modulus at the end of $\mu_A(t)$] to $4\rho RT/5M_e$ in $G(t)$. The relaxation time of the $\mu_X(t)$ process, τ_X, decreases linearly with decreasing molecular weight. The τ_X for the PEB-2 sample with $M_w=1.9\times10^5$ is estimated to be about 100 times larger than τ_1^e;[39] any effect that can come from $\mu_X(t)$ should be far beyond the time windows of the DSF measurements. In other words, the PEB-2 sample with $M_w=1.9\times10^5$ may be considered as a well-entangled system suitable for comparing its neutron spin-echo results with Eq. (7). As observed in the study of a series of PEB-2 samples,[40] when the molecular weight is low enough, the heights of the plateaus at different q values drop more and the slopes on the plateaus are enhanced with decreasing molecular weight. These symptoms suggest an effect involving the $\mu_X(t)$ process, which relaxes the fixed-end assumption more with decreasing molecular weight. In particular, at $M_w=1.24\times10^4$ (the smallest molecular weight studied in Ref. 40), the τ_X value is only about six times τ_1^e; the effect of $\mu_X(t)$ is well within the time windows of the DSF measurements. Thus, as expected, considerable drops in the heights of the plateaus are observed in the case of the sample with $M_w=1.24\times10^4$.

VI. DISCUSSION

A. The *q*-split plateaus and the boundary conditions

As opposed to Eq. (7) being for strands with both ends fixed, Eq. (5) is for chains free at both ends, yet trapped in a domain with a diameter of $\sqrt{N_0}b$. Here we compare Eqs. (5) and (7) under the situation that the domain diameter for the former is the same as the entanglement length for the latter, namely, $a=\sqrt{N_e}b=\sqrt{N_0}b$. As shown in Appendix D, both Eqs. (5) and (7) converge to the same limiting form [Eq. (D3)] in the time region of $t\ll\tau_1$ or τ_1^e (τ_1 and τ_1^e are the same as N_0 and N_e are treated as equivalent here) for $qa\gg1$ (or $qa>10$). However, in the region $\sim7>qa>\sim1$, Eq. (5) gives a very different distribution of q-split plateaus from Eq. (7) (Figs. 2 and 3). The comparison of Eqs. (D1) and (D2) indicates that in the short-time region, Eqs. (5) and (7) converge to the limiting form [Eq. (D3)] from the opposite sides (see Fig. 3). As opposed to Eq. (7) being successful, as shown in Sec. V, Eq. (5) is far from being able to describe the experimental results. The drastic differences between Eqs. (5) and (7) indicate that the fixed-end boundary conditions are an essential ingredient—confinement alone is not sufficient—for the observed distribution of the q-split plateaus. This conclusion logically leads to the mechanism of *chain slippage* through entanglement links as pictured in the Doi–Edwards model—as a chain conformation, say, deformed, has to relax completely eventually without involving a chain break-and-link process. Extensive studies[1,2,7–12,41–44] of polymer viscoelastic responses—including the successful prediction of the damping factor in the studies of nonlinear viscoelasticity[1,2,41–44]—have supported the slip-link picture as embodied in the Doi–Edwards model.[1,2,26] The analyses of the spin-echo results as presented in this paper further support the model on the microscopic level.

B. Comparisons with existing models

Models have been developed for understanding the coherent dynamic scatterings of single entangled chains by de Gennes,[45] Ronca,[46] and des Cloizeaux.[47] These theories have been used to explain the q-split plateaus with different degrees of success; performances of these theories have been compared.[6,24,48] As de Gennes' theory has often been used for data analyses in the literature and appears to give the entanglement length closest to the rheological value among the three theories, we shall mainly focus on its comparison with Eq. (7).

de Gennes' theory and Eq. (7) are based on different starting points: As opposed to the fixed-end boundary conditions for each entanglement strand in the latter case, de Gennes' theory imposes a tensile force $3kT/a$ (as given by the Doi–Edwards theory[1,2,26] for maintaining the primitive-chain contour length $L=R^2/a$) on both ends of the chain. de Gennes' theory considers fluctuations of the segmental density along the primitive chain, which has the average value given by $N_0/L=N_e/a=N_e^{0.5}/b$, and terms it as "local reptation." The sort of process considered by deGennes is physically similar to those responsible for the $\mu_X(t)$ and $\mu_B(t)$ processes in the ERT.[2,7–12] The local reptation is regarded in de Gennes' theory as responsible for the main dynamics observed in the coherent scattering from one reptating chain, if the chain is extremely well entangled. Both the present proposed Rouse–Mooney model and de Gennes' picture expect that, given enough time, reptation will eventually be fully carried out randomizing the whole primitive chain or tube. The main difference between the two is that the former focuses on the dynamics within one step length of the primitive chain as opposed to the latter being intended for dynamics beyond one step length. In de Gennes' picture, the slip-link "structure" and the existence of the Rouse–Mooney process (including chain motions perpendicular to the primitive path) before chain slippage has the chance to take place are ignored. In accord with this picture, the condition $q^2a^2\ll1\ll q^2R^2$ has been used at several approximation steps in the derivation of de Gennes' theoretical result.

After making additional approximations, de Gennes obtained a DSF function consisting of two separate terms:

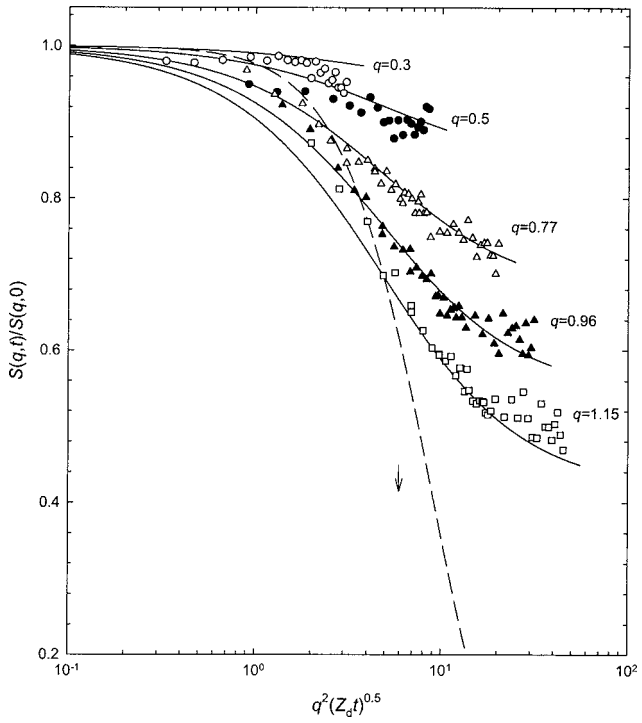

FIG. 9. Comparison of the normalized DSF results (○, ●, △, ▲, and □ at q=0.3, 0.5, 0.77, 0.96, and 1.15 nm^{-1}, respectively) of the PEB-2 sample with the curves calculated from de Gennes' equation (with a=4.9 nm), both expressed as a function of the reduced Rouse variable, $q^2(Z_dt)^{1/2}$. The comparison is made with Z_d=7 nm^4 ns^{-1}. The limiting curve for $qa\rightarrow\infty$ [Eq. (D3)] is shown as the dashed line. The arrow marks the position of $q^2(Z_d\tau_q)^{1/2}$=6.

A time-dependent term characterized by the time constant $\tau_q=36/Z_dq^4$—independent of the length scale a—is to account for the relaxation in the short-time region. The other term (the so-called creep term), which can justifiably be regarded as time independent for a well-entangled sample, is responsible for the existence of plateaus at long times.

The comparisons of the experimental results of the PEB-2 sample with de Gennes' equation as well as with Eq. (D3) are shown in Fig. 9.[49] The comparisons at different q values are made using the same values of Z_d (=7 nm^4/ns)[24,35] and a (=4.9 nm) as obtained by Wischnewski and Richter (Fig. 1 of Ref. 24) for giving an "optimum" fit. Note this Z_d value and that used in the comparison with Eq. (7) shown in Fig. 8 are equal, both being consistent with the incoherent scattering results.[38] With a=4.9 nm, the results shown in Fig. 9 cover the range from qa=1.47 to 5.64 as opposed to the condition $q^2a^2\ll1\ll q^2R^2$ required in the development of de Gennes' theory. This represents a fundamental inconsistency that would undermine the soundness of the analysis in terms of de Gennes' theory.

The characteristic time in de Gennes' equation is located at the fixed position $q^2(Z_d\tau_q)^{1/2}$=6 in Fig. 9 as opposed to the position of the relaxation time of the lowest Rouse–Mooney mode, as given by $q^2(Z_d\tau_1^e)^{1/2}=q^2a^2/\pi$, moving to the right side with increasing q in Fig. 8. These positions are indicated by arrows in Figs. 8 and 9. To a large degree due to this difference, while the curves calculated from Eq. (7) move closer to Eq. (D3) with increasing q over the range $1\sim4>q^2(Z_dt)^{0.5}>0.1$, the curves calculated from de Gennes' equation deviate more from it. This contrast represents a gap between the short-time and long-time regions in de Gennes' theory. Thus, Richter *et al.*[24,35,38,48] have resorted to Eq. (D3) to determine the Z_d value needed in comparing the experimental results with de Gennes' equation emphasizing comparisons over the long-time region where the q-split plateaus occur. The difference between using Eq. (D3) and using Eq. (7) to determine the Z_d value and its consequence for drawing conclusion have been analyzed and discussed in detail in Sec. V A for the PVE sample. The discussed gap is very much responsible for the large deviations of the experimental results on the high side from de Gennes' equation over the short-time region at q=0.96 and 1.15 nm^{-1} and on the low side at q=0.3 and 0.5 nm^{-1} as can be clearly observed in Fig. 9. Including the plateau regions, unlike in the comparison between experiment and Eq. (7), the observed deviations from de Gennes'equation do not appear to be systematic at different q values. This may be unavoidable due to the inconsistency between the range of qa as emerging from the analysis-obtained results and that covered by de Gennes' theory.

The natural reduction of Eq. (7) to Eq. (D3) allows us to display a full range of DSF curves as a function of the reduced Rouse variable $q^2(Z_dt)^{1/2}$ in a unified way as shown in Fig. 3. This is a property not shared by the other theories. The shown full range forms a framework or "map," with respect to which different regions of the DSF curves at different q values can be located and studied in a consistent manner. One may notice that the Langevin equation and normal modes involved in deriving Eq. (7) are the same as in deriving the $\mu_A(t)$ relaxation process[2,10] as part of the ERT. Thus, data analyses in terms of Eq. (7) can benefit directly from the past studies of polymer viscoelasticity in terms of the ERT.[2,7–12]

The entanglement length a calculated from the plateau modulus G_N has been regarded as a characteristic quantity related to entanglement. It has been well established that the number of entanglement strands per cubed entanglement length n_t is a universal constant.[2,33,50,51] In addition to the theoretical distinctions of Eq. (7) pointed out above, the a value obtained from analyzing the DSF results of the PEB-2 sample in terms of Eq. (7) is closer to the rheological value than in terms of the other theories. For PEB-2 at 509 K, the a values obtained from the various analyses[24,48] are 4 nm [Eq. (7)], 4.6–4.9 nm (de Gennes), 4.74 nm (Ronca), and 5.98 nm (des Cloiseaux) versus the rheological value of 3.44 nm at 413 K.[2,33,51] Exempt from effects of the slower ERT modes of motion $\mu_X(t)$, $\mu_B(t)$, and $\mu_C(t)$, a likely reason for the a value of a well-entangled system obtained from analyses in terms of Eq. (7) to be slightly higher than the rheological value is the temperature difference. For instance, in the case of PEB-17.6 [poly(ethylene-co-bulene) with 17.6 ethyl branches per 100 carbons],[2,33,51] calculations from the plateau modulus values give a=4.71 nm at 413 K and a =3.75 nm at 298 K. This example suggests that an ~100 K difference in temperature can cause a difference in the a value as large as 25%. Such an effect may be responsible for the difference between 4 nm at 509 K as obtained from ana-

lyzing the DSF curves in terms of Eq. (7) and the rheological value of 3.44 nm at 413 K for the PEB-2 polymer.

VII. SUMMARY

The theoretical DSF function forms based on the Rouse and Rouse–Mooney models, both discrete and continuous, are given and their calculated results are compared in this paper. It has been shown that it is sufficient to use the continuous Rouse–Mooney model to analyze the coherent neutron scatterings from single well-entangled chains in the q region where a Rouse-segment-based theory is applicable. In the analyses, $a=\sqrt{N_e}b$ and $Z_d=3kTb^2/\zeta$ are the only adjustable parameters, wherein for all practical purposes, an arbitrary pair of sufficiently large N_e and small b may be chosen (Appendix B).

Two characteristics are identified in the DSF functional form for well-entangled single chains [Eq. (7)]: One is the deviations from the limiting form [Eq. (D3)] in the region $\sim 4 > q^2(Z_d t)^{0.5} > \sim 0.1$ (corresponding to a time region from $t \ll \tau_1^e$ to $t < \tau_1^e$) to the faster side as qa is in the range 1–5. The other is the q-split plateaus that can be experimentally observed in the time region $t > \tau_1^e$ when qa is between ~ 1 and ~ 7, allowing a high-resolution determination of the a value. The validity of these two characteristics is well supported by the comparisons between theory and experiment at different q values in the respective regions. The entanglement length a extracted from analyzing the DSF line shapes of the studied well-entangled PEB-2 polymer is in agreement with the rheological value within 20%. It is shown that the small difference may be due to the large difference between the temperatures at which the two values are respectively determined.

From this study, it is shown that the fixed-end boundary conditions assumed for the dynamic behavior of a well-entangled entanglement strand are essential for obtaining the distribution of the q-split plateaus as observed experimentally by the neutron spin-echo spectroscopy. This strongly supports that the Rouse–Mooney model is applicable microscopically as it has been shown to be so macroscopically in the studies of viscoelastic-response functions.[2,7–12] This also represents a support on the microscopic level for the mechanism of chain slippage through entanglement links as embodied in the Doi–Edwards theory.

Equation (7) reduces to the limiting form Eq. (D3) naturally allowing a full range of DSF curves to be presented in terms of the reduced Rouse variable $q^2(Z_d t)^{1/2}$ in a unified way. The displayed full range represents a framework or map, with respect to which different regions of DSF may be located and studied in a consistent manner.

ACKNOWLEDGMENTS

This work is supported by the National Science Council (NSC 96-2113-M-009-020-MY3). We thank Professor Richter and Professor Colmenero for providing us with the neutron spin-echo data of the PEB-2, PIB, and PVE samples.

APPENDIX A: THE DISCRETE ROUSE AND ROUSE–MOONEY MODELS

The DSF based on the discrete Rouse model is given by[52]

$$S(\mathbf{q},t)=\frac{1}{N_0}\exp(-\mathbf{q}^2D_Gt)\times\sum_{n=1}^{N_0}\sum_{m=1}^{N_0}\exp\left[-\frac{\mathbf{q}^2}{6}b^2|m-n|-\frac{2\mathbf{q}^2b^2}{3N_0}\sum_{p=1}^{N_0-1}f(m,p,N_0)f(n,p,N_0)\times\left[1-\exp\left(\frac{-t}{\tau_p}\right)\right]\right], \tag{A1}$$

where

$$D_G=\frac{kT}{N_0\zeta}, \tag{A2}$$

$$f(m,p,N_0)=\sum_{s=1}^{N_0-1}\frac{s}{N_0}\sin\left(\frac{sp\pi}{N_0}\right)-\sum_{s=m}^{N_0-1}\sin\left(\frac{sp\pi}{N_0}\right), \tag{A3}$$

and

$$\tau_p=K\frac{\pi^2M^2}{12N_0^2\sin^2(p\pi/2N_0)},\quad p=1,2,3,\ldots,N_0-1. \tag{A4}$$

The DSF of the discrete Rouse–Mooney model is given by[52]

$$S(\mathbf{q},t)=\frac{1}{N_e}\times\sum_{n=1}^{N_e}\sum_{m=1}^{N_e}\exp\left[-\frac{\mathbf{q}^2}{6}b^2|m-n|-\frac{\mathbf{q}^2b^2}{6N_e}\sum_{p=1}^{N_e-1}h(m,p,N_e)h(n,p,N_e)\times\left[1-\exp\left(\frac{-t}{\tau_p^e}\right)\right]\right], \tag{A5}$$

with

$$h(m,p,N_e)=\frac{\sin\left(\frac{mp\pi}{N_e}\right)}{\sin\left(\frac{p\pi}{2N_e}\right)} \tag{A6}$$

and

$$\tau_p^e=K\frac{\pi^2M_e^2}{12N_e^2\sin^2(p\pi/2N_e)},\quad p=1,2,3,\ldots,N_e-1. \tag{A7}$$

As expected, when $N_0\to\infty$ or $N_e\to\infty$, Eqs. (A1) and (A5) reduce to Eqs. (2) and (7), respectively, and Eqs. (A4) and (A7) to Eqs. (3) and (8), respectively.

APPENDIX B: DYNAMIC PARAMETERS IN ROUSE-SEGMENT-BASED THEORIES

In a Rouse-segment-based theory (the Rouse theory or the ERT), the relaxation times can be expressed as a product of the frictional factor K and a structural factor,[2,7–12] which is a function of molecular weight M and/or entanglement mo-

lecular weight M_e. From analyzing the viscoelastic results in terms of a Rouse-segment-based theory, K is the key dynamic parameter that can be extracted. For instance, in the case of using the ERT to analyze the viscoelastic responses: $G(t)$ and $J(t)$ of entangled nearly monodisperse polystyrene melts, the obtained K values [for the $\mu_X(t/\tau_X)$, $\mu_B(t/\tau_B)$, and $\mu_C(t/\tau_C)$ processes] are independent of molecular weight as expected from the theory (see Table 1 of Ref. 7).[2,7–11] From analyzing the $G(t)$ and $G^*(\omega)$ line shapes of entangled polystyrene binary-blend solutions in terms of the linear combination of the ERT and the Rouse theory, the values of K as embodied in the two theories have been found to agree within 20%.[2,9,12] Very importantly, this agreement indicates that the Rouse theory and the ERT have the same footing at the Rouse-segmental level. [Note that the frictional factor for the Rouse–Mooney process $\mu_A(t/\tau_A)$, denoted by K', is larger than K by a factor $R_K(M/M_e)$ that depends on the normalized molecular weight M/M_e. As detailed in Refs. 2, 9, 11, and 12, $R_K(M/M_e)$ being greater than 1—declining from the plateau value of 3.3 at $M/M_e>10$ to the limiting value 1 as $M/M_e\to 1$—represents dynamic anisotropy due to topological constraint of entanglements. The following discussion on K is also applicable to K'.]

Here, we would like to show that the frictional factor K is equivalent to the parameter Z_d that has often been extracted from the coherent dynamic neutron scattering studies. The entanglement distance a can be expressed as

$$a^2 = K_\infty M_e, \tag{B1}$$

where K_∞ is defined as the ratio of the mean square end-to-end distance of a polymer to its molecular weight, $K_\infty = R^2/M$, which can be determined by static neutron scattering.[1,2,33,50,51] One may also write

$$a^2 = N_e b^2 = \frac{M_e}{m} b^2. \tag{B2}$$

The combination of Eqs. (B1) and (B2) leads to

$$b^2 = K_\infty m. \tag{B3}$$

Since K_∞ is a constant, b^2 is linearly proportional to m. Using this relation, Eq. (4) is obtained.

As being inversely proportional to K [Eq. (4)], Z_d may replace K playing the role of the key dynamic parameter. Even though in the neutron spin-echo studies of polymers, the continuous Rouse model is always used as in this study, Z_d theoretically remains the relevant key dynamic parameter because of the scaling relations $\zeta \propto m$ and $b^2 \propto m$. For example, Eq. (D3) is a universal function of $q^2(Z_d t)^{1/2}$.

APPENDIX C: THE BASIC DSF FORM OF A WELL-ENTANGLED CHAIN UNDER THE CONDITION $qR \gg 1$

In a well-entangled labeled chain, as the entanglement points (slip links) are regarded as fixed, the modes of motion of an entanglement strand are isolated from those of others, and segments belonging to different entanglement strands are not correlated. Denoting entanglement strands by k and l, and beads by n and m, the DSF of the labeled chain can be reduced as follows:

$$\begin{aligned} S(\mathbf{q},t) &= \frac{1}{N_0}\sum_{k=1}^{N}\sum_{l=1}^{N}\sum_{n=1}^{N_e}\sum_{m=1}^{N_e}\langle \exp[i\mathbf{q}\cdot(\mathbf{R}_n^k(t)-\mathbf{R}_m^l(0))]\rangle \\ &= \frac{1}{N_0}\sum_{k=1}^{N}\sum_{n=1}^{N_e}\sum_{m=1}^{N_e}\langle \exp[i\mathbf{q}\cdot(\mathbf{R}_n^k(t)-\mathbf{R}_m^k(0))]\rangle + \frac{1}{N_0}\sum_{k=1}^{N}\sum_{l\neq k}^{N}\left\langle \sum_{n=1}^{N_e}\exp(i\mathbf{q}\cdot\mathbf{R}_n^k(t))\right\rangle\left\langle \sum_{m=1}^{N_e}\exp(-i\mathbf{q}\cdot\mathbf{R}_m^l(0))\right\rangle \\ &= \frac{N}{N_0}\sum_{n=1}^{N_e}\sum_{m=1}^{N_e}\langle \exp[i\mathbf{q}\cdot(\mathbf{R}_n(t)-\mathbf{R}_m(0))]\rangle + \frac{1}{N_0}\left\langle \sum_{k=1}^{N}\sum_{n=1}^{N_e}\exp(i\mathbf{q}\cdot\mathbf{R}_n^k(t))\right\rangle\left\langle \sum_{l=1}^{N}\sum_{m=1}^{N_e}\exp(-i\mathbf{q}\cdot\mathbf{R}_m^l(0))\right\rangle \\ &\quad - \frac{1}{N_0}\sum_{k=1}^{N}\left\langle \sum_{n=1}^{N_e}\exp(i\mathbf{q}\cdot\mathbf{R}_n^k(t))\right\rangle\left\langle \sum_{m=1}^{N_e}\exp(-i\mathbf{q}\cdot\mathbf{R}_m^k(0))\right\rangle. \end{aligned} \tag{C1}$$

Because at any moment, the beads $\{\mathbf{R}_n(t)\}$ are distributed randomly over $R \gg q^{-1}$, the second and third terms of Eq. (C1) are negligible, and Eq. (C1) reduces to the form given by Eq. (6).

APPENDIX D: LIMITING DSF FORM IN THE SHORT-TIME REGION WHEN $q^2N_0b^2$ OR $q^2N_eb^2 \gg 1$

When $\mathbf{q}^2N_0b^2$ or $\mathbf{q}^2N_eb^2 \gg 1$, we may limit consideration to the time region $t \ll \tau_1$ in Eq. (5) [equivalently in Eq. (2), as D_G is very small and $\exp(-q^2D_Gt)$ is practically equal to 1 in the short-time region] or $t \ll \tau_1^e$ in Eq. (7), respectively. In the short-time domain, the respective summations over p in the exponents of these equations are dominated by large p. Under p being large, the underlined terms in the factors

$$2\cos\left(\frac{p\pi m}{N_0}\right)\cos\left(\frac{p\pi n}{N_0}\right) = \cos\left(\frac{(n-m)p\pi}{N_0}\right) + \underline{\cos\left(\frac{(n+m)p\pi}{N_0}\right)} \tag{D1}$$

and

$$2\sin\left(\frac{p\pi m}{N_e}\right)\sin\left(\frac{p\pi n}{N_e}\right)=\cos\left(\frac{(n-m)p\pi}{N_e}\right)-\cos\left(\frac{(n+m)p\pi}{N_e}\right) \tag{D2}$$

as, respectively, embodied in Eqs. (2) [or Eq. (5)] and (7) change sign rapidly, and their contributions become very small and negligible. Thus, Eqs. (2) [or Eq. (5)] and (7) lead to the same result. By replacing the summations over m and n by integrations and using the fact that the integrand has a sharp peak at $n \cong m$, the following limiting form can be derived:[1]

$$S(\mathbf{q},t)=\frac{12}{q^2b^2}\int_0^\infty du\,\exp\{-u-(t/\tau_q)^{1/2}h(u(t/\tau_q)^{-1/2})\}, \tag{D3}$$

where

$$\tau_q=\frac{12\zeta}{kTq^4b^2}=\frac{36}{Z_dq^4} \tag{D4}$$

and

$$h(u)=\frac{2}{\pi}\int_0^\infty dx\frac{\cos(xu)}{x^2}(1-\exp(-x^2)). \tag{D5}$$

[1] M. Doi and S. F. Edwards, *The Theory of Polymer Dynamics* (Oxford University Press, Oxford, 1986).
[2] Y.-H. Lin, *Polymer Viscoelasticity: Basics, Molecular Theories, and Experiments* (World Scientific, Singapore, 2003).
[3] J. D. Ferry, *Viscoelastic Properties of Polymers*, 3rd ed. (Wiley, New York, 1980).
[4] Y. Imanishi, K. Adachi, and T. Kotaka, J. Chem. Phys. **89**, 7593 (1988).
[5] D. Boese and F. Kremer, Macromolecules **23**, 829 (1990).
[6] D. Richter, M. Monkenbusch, A. Arbe, and J. Colmenero, Adv. Polym. Sci. **174**, 1 (2005).
[7] Y.-H. Lin, J. Phys. Chem. B **109**, 17654 (2005).
[8] Y.-H. Lin, J. Phys. Chem. B **109**, 17670 (2005).
[9] Y.-H. Lin, J. Phys.: Condens. Matter **19**, 466101 (2007).
[10] Y.-H. Lin, Macromolecules **17**, 2846 (1984).
[11] Y.-H. Lin, Macromolecules **19**, 159 (1986).
[12] Y.-H. Lin, Macromolecules **20**, 885 (1987).
[13] P. E. Rouse, Jr., J. Chem. Phys. **21**, 1272 (1953).
[14] R. B. Bird, C. F. Curtiss, R. C. Armstrong, and O. Hassager, *Dynamics of Polymeric Liquids*, 2nd ed. (Wiley, New York, 1987), Vol. 2.
[15] Y.-H. Lin, Macromolecules **19**, 168 (1986).
[16] Y.-H. Lin and J.-H. Juang, Macromolecules **32**, 181 (1999).
[17] D. J. Plazek, J. Phys. Chem. **69**, 3480 (1965).
[18] D. J. Plazek, J. Polym. Sci., Part A-2 **6**, 621 (1968).
[19] D. J. Plazek and V. M. O'Rourke, J. Polym. Sci., Part A-2 **9**, 209 (1971).
[20] T. Inoue, T. Onogi, M.-L. Yao, and K. Osaki, J. Polym. Sci., Part B: Polym. Phys. **37**, 389 (1999).
[21] M. Mooney, J. Polym. Sci. **34**, 599 (1959).
[22] D. Richter, M. Monkenbusch, J. Allgeier, A. Arbe, J. Colmenero, B. Farago, Y. Cheol Bae, and R. Faust, J. Chem. Phys. **111**, 6107 (1999).
[23] W. Paul, G. D. Smith, D. Y. Yoon, B. Farago, S. Rathgeber, A. Zirkel, L. Willner, and D. Richter, Phys. Rev. Lett. **80**, 2346 (1998).
[24] A. Wischnewski and D. Richter, Europhys. Lett. **52**, 719 (2000).
[25] D. A. McQuarie, *Statistical Mechanics* (Harper & Row, New York, 1976).
[26] M. Doi and S. F. Edwards, J. Chem. Soc., Faraday Trans. 2 **74**, 1789 (1978); **74**, 1802 (1978).
[27] M. Doi, J. Polym. Sci., Polym. Phys. Ed. **18**, 1005 (1980).
[28] Y.-H. Lin and A. K. Das, J. Chem. Phys. **126**, 074902 (2007).
[29] Y.-H. Lin and A. K. Das, J. Chem. Phys. **126**, 074903 (2007).
[30] T. Inoue and K. Osaki, Macromolecules **29**, 1595 (1996).
[31] T. Inoue, H. Okamoto, and K. Osaki, Macromolecules **24**, 5670 (1991).
[32] H. Okamoto, T. Inoue, and K. Osaki, J. Polym. Sci., Part B: Polym. Phys. **33**, 417 (1995).
[33] Y.-H. Lin, *Polymer Viscoelasticity: Basics, Molecular Theories, and Experiments* (Ref. 2), Table 13.1 or 13.2 and references therein.
[34] P. G. de Gennes, Physics **3**, 37 (1967).
[35] D. Richter, B. Farago, R. Buters, L. J. Fetters, J. S. Huang, and B. Ewen, Macromolecules **26**, 795 (1993).
[36] D. Richter, M. Monkenbusch, L. Willner, A. Arbe, J. Colmenero, and B. Farago, Europhys. Lett. **66**, 239 (2004).
[37] The Z_d values are obtained from our least-squares fittings of Eq. (9) to the data at different q values shown in Fig. 2 of Ref. 36.
[38] A. Wischnewski, M. Monkenbusch, L. Willner, D. Richter, and G. Kali, Phys. Rev. Lett. **90**, 058302 (2003).
[39] The $R_K(M/M_e)$ (see Appendix B) value of 3.3 obtained for polystyrene at high molecular weights is used in the estimation of the ratio τ_X/τ_1^e.
[40] A. Wischnewski, M. Monkenbusch, L. Willner, D. Richter, A. E. Likhtmann, T. C. B. McLeish, and B. Farago, Phys. Rev. Lett. **88**, 058301 (2002).
[41] K. Osaki and M. Kurata, Macromolecules **13**, 671 (1980).
[42] K. Osaki, K. Nishizawa, and M. Kurata, Macromolecules **15**, 1068 (1982).
[43] C. M. Vrentas and W. W. Graessley, J. Rheol. **26**, 359 (1982).
[44] Y.-H. Lin, J. Non-Newtonian Fluid Mech. **23**, 163 (1987).
[45] P. G. deGennes, J. Phys. (Paris) **42**, 735 (1981).
[46] G. J. Ronca, J. Chem. Phys. **79**, 1031 (1983).
[47] J. des Cloizeaux, J. Phys. I **3**, 1523 (1993).
[48] P. Schleger, B. Farago, C. Lartigue, A. Kollmar, and D. Richter, Phys. Rev. Lett. **81**, 124 (1998).
[49] Here, we ignore the difference between "reptation" and "local reptation" defined in Refs. 24 and 48, as the difference is very small particularly for the extremely well-entangled system, PEB-2 sample with $M_w=1.9\times10^5$, studied here. The time-independent term in de Gennes' original version has the form $1-q^2a^2/36$; however, it has been replaced by $\exp(-q^2a^2/36)$ in the data analyses as reported in Refs. 24 and 48. For qa being smaller than ~3.5, one form is a good approximation to the other.
[50] Y.-H. Lin, Macromolecules **20**, 3080 (1987).
[51] L. J. Fetters, D. J. Lohse, D. Richter, T. A. Witten, and A. Zirkel, Macromolecules **27**, 4639 (1994).
[52] Y.-H. Lin (unpublished).